

High Chloride Doping Levels Stabilize the Perovskite Phase of Cesium Lead Iodide

Subham Dastidar,[†] David A. Egger,[‡] Liang Z. Tan,[§] Samuel B. Cromer,[†] Andrew D. Dillon,[†] Shi Liu,^{||} Leeor Kronik,[‡] Andrew M. Rappe,[§] and Aaron T. Fafarman^{*,†}

[†]Department of Chemical and Biological Engineering, Drexel University, 3141 Chestnut Street, Philadelphia, Pennsylvania 19104, United States

[‡]Department of Materials and Interfaces, Weizmann Institute of Science, Rehovoth 76100, Israel

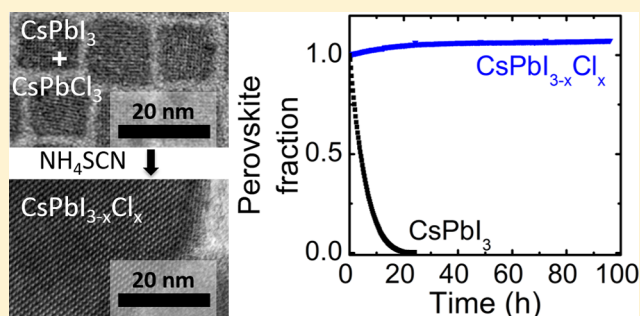
[§]The Makineni Theoretical Laboratories, Department of Chemistry, University of Pennsylvania, Philadelphia, Pennsylvania 19104–6323, United States

^{||}Geophysical Laboratory, Carnegie Institution for Science, Washington, DC 20015, United States

Supporting Information

ABSTRACT: Cesium lead iodide possesses an excellent combination of band gap and absorption coefficient for photovoltaic applications in its perovskite phase. However, this is not its equilibrium structure under ambient conditions. In air, at ambient temperature it rapidly transforms to a nonfunctional, so-called yellow phase. Here we show that chloride doping, particularly at levels near the solubility limit for chloride in a cesium lead iodide host, provides a new approach to stabilizing the functional perovskite phase. In order to achieve high doping levels, we first co-deposit colloidal nanocrystals of pure cesium lead chloride and cesium lead iodide, thereby ensuring nanometer-scale mixing even at compositions that potentially exceed the bulk miscibility of the two phases. The resulting nanocrystal solid is subsequently fused into a polycrystalline thin film by chemically induced, room-temperature sintering. Spectroscopy and X-ray diffraction indicate that the chloride is further dispersed during sintering and a polycrystalline mixed phase is formed. Using density functional theory (DFT) methods in conjunction with nudged elastic band techniques, low-energy pathways for interstitial chlorine diffusion into a majority-iodide lattice were identified, consistent with the facile diffusion and fast halide exchange reactions observed. By comparison to DFT-calculated values (with the PBE exchange-correlation functional), the relative change in band gap and the lattice contraction are shown to be consistent with a Cl/I ratio of a few percent in the mixed phase. At these incorporation levels, the half-life of the functional perovskite phase in a humid atmosphere increases by more than an order of magnitude.

KEYWORDS: Air-stability, chemical sintering, ligand exchange, colloidal nanocrystal doping, nudged elastic band, halide exchange



The hybrid, organic/inorganic lead halide perovskites¹ have generated tremendous interest in the photovoltaic community due to their astonishingly rapid improvements in power conversion efficiency,² currently greater than 20%,³ and their amenability to simple, low-cost, solution-based fabrication.⁴ These materials have the formula ABX₃, and in the prototypical composition, A is methylammonium (MA) or formamidinium, B is lead, and X is iodide (e.g., MAPbI₃). However, the organic component is highly hygroscopic,^{5,6} volatile,⁷ and subject to chemical decomposition, particularly acid dissociation.⁸ By replacing the organic component with cesium at the A-site, an all-inorganic perovskite can be formed, obviating the problems of volatility and chemical decomposition. CsPbI₃ was known since the 1950s as a semiconductor with a band gap near the red edge of the visible spectrum.⁹ However, until very recently¹⁰ it was passed over for

photovoltaic applications because the perovskite phase has been found to be unstable under ambient conditions. It is formed at high temperature, conditions in which the cubic perovskite geometry (Figure 1a) is the equilibrium phase. However, in air at room temperature the black CsPbI₃ undergoes a rapid phase-transition to a nonfunctional, non-perovskite structure, known as the “yellow phase”.^{9,11–13} Unlike the cubic (or distorted cubic) perovskite structure in which the metal–halide octahedra share corners, the orthorhombic yellow phase is comprised of 1D chains of edge-sharing octahedra, as found in the canonical NH₄CdCl₃ structure (Figure 1b). Nonetheless, the first examples of CsPbI₃ solar cells show

Received: February 12, 2016

Revised: April 28, 2016

Published: May 2, 2016



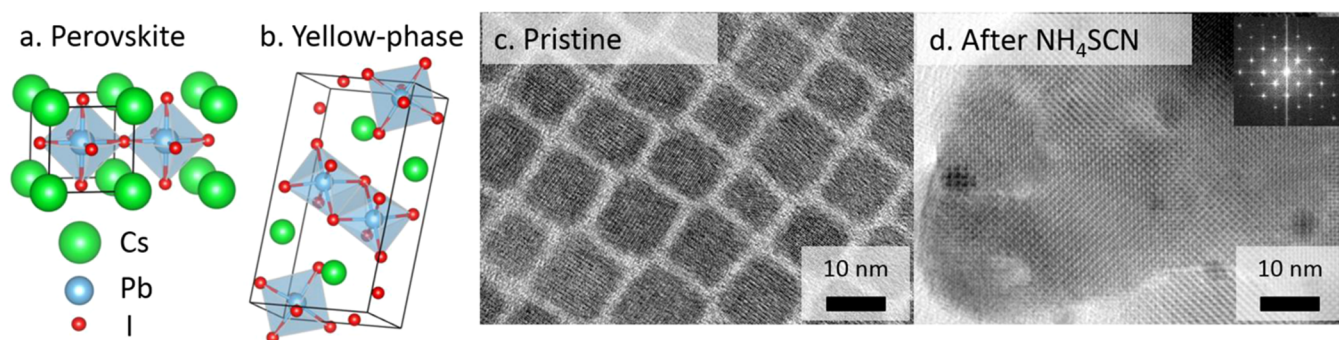


Figure 1. Sketch of the (a) perovskite and (b) yellow-phase crystal forms of CsPbI_3 . TEM images of a film of CsPbI_3 perovskite nanocrystals before (c) and after (d) ligand removal by immersion in a solution of NH_4SCN at 23 °C. Inset shows the Fourier transform of the image.

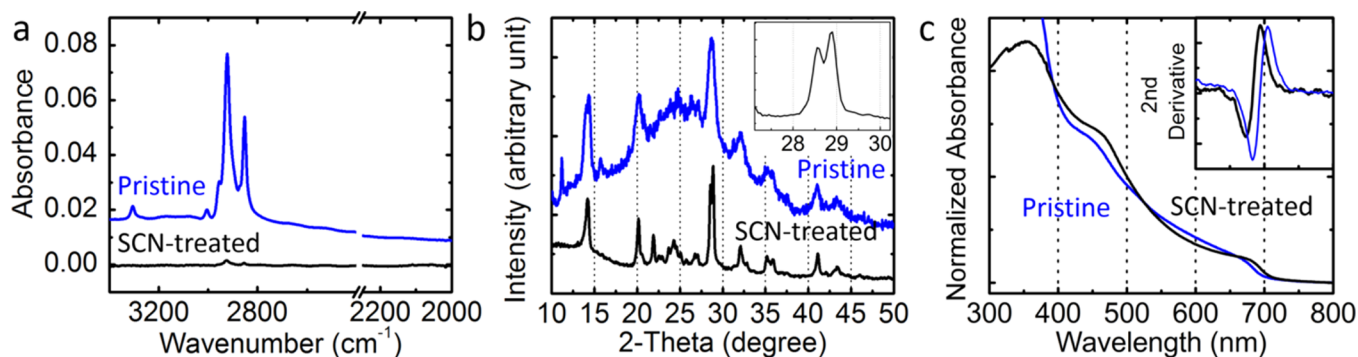


Figure 2. Spectroscopic and structural characterization of CsPbI_3 perovskite nanocrystal solid films before (blue) and after (black) treatment with NH_4SCN . (a) FTIR absorbance spectra. (b) XRD with inset focusing on the split (200) peak. (c) UV-vis absorbance spectra. Inset shows the second derivative of the absorbance spectrum, in the range of 600–800 nm, highlighting the band shifting and narrowing upon SCN treatment.

promise,^{10,14} and earlier work employing the more stable CsPbBr_3 as a photovoltaic absorber layer demonstrated comparable efficiency to its hybrid equivalent, MAPbBr_3 .¹⁵ Recently, it has been shown that doping the hybrid perovskites with cesium can enhance their stability without severely impacting their performance.^{16–22}

Motivated by the robust phase stability observed for CsPbCl_3 ,^{9,23} we hypothesized that the stability of CsPbI_3 would be improved by incorporating chloride as a dopant. In the closely related MAPbI_3 , it is known that the presence of chloride during the synthesis enhances its air stability.^{4,24} However, the mechanism of this enhancement is unknown, and further even the extent of chloride incorporation into the MAPbI_3 phase is debated.^{25–31} In contrast, bromide and iodide form solid solutions at all mole ratios in CsSnX_3 ,³² CsPbX_3 ,³³ and MAPbX_3 ,^{6,34} and the $\text{MAPbI}_{3-x}\text{Br}_x$ mixed crystal has recently been shown to be more stable than the pure iodide phase.³⁴ Despite widespread interest in the properties of the $\text{MAPbI}_{3-x}\text{Cl}_x$ mixed crystal,^{4,25,26,29,35} chloride appears to have limited miscibility in iodide-perovskites, as observed for CsSnI_3 ³⁶ and MAPbI_3 ,^{25,31,37} perhaps due to the size mismatch between chloride and iodide. The miscibility of chloride in a majority CsPbI_3 phase has been less well studied, though recent studies of CsPbX_3 nanomaterials, discussed below, suggest that it is similarly low.^{33,38,39} To the best of our knowledge, thin films of perovskite-phase $\text{CsPbI}_{3-x}\text{Cl}_x$ have not been synthesized prior to this study. To synthesize these materials, we introduce the following two-step process. We first deposit a colloidal mixture of CsPbI_3 and CsPbCl_3 perovskite nanocrystals onto a substrate. In this manner a nanocrystal solid is formed, consisting of CsPbI_3 nanocrystals, substitutionally

doped with CsPbCl_3 nanocrystals. We then use a chemical agent to induce nanocrystal sintering and grain growth at room temperature. This process ensures nanoscale mixing of these otherwise low miscibility components and provides the possibility of further, atomic-scale mixing during the sintering step. In contrast, a traditional synthetic approach using molecular precursors requires high temperatures for crystal formation,^{10,15} which could have the undesirable effect of promoting phase separation of the chloride dopant. An important feature of our approach is that the spectroscopically distinct signatures of the two different nanocrystal constituents provide critical insight into the composition and structure of the films throughout the process. Density functional theory (DFT) is applied to understand the origins of the facile, room-temperature intermixing that we observe experimentally and to interpret band shifts and lattice parameter changes as a function of doping.

Results and Discussion. Colloidal nanocrystals of perovskite-phase CsPbCl_3 and CsPbI_3 are synthesized by the route described by the Kovalenko group,³³ yielding cubes that are approximately 10 nm to a side, as shown in Figure 1c. As synthesized, they are capped with organic capping groups (or “ligands”) that passivate the surface and allow the nanocrystals to be dispersed in organic solvents. The colloidal dispersions are drop-cast or spin-cast onto a substrate. By immersing the coated substrates in a solution of NH_4SCN in isopropanol at room temperature, these ligands are removed. As shown in the Fourier transform infrared (FTIR) absorbance spectra in Figure 2a, the C–H stretching transitions at 2900 cm^{-1} associated with the original organic ligands (blue curve) are absent after treatment with NH_4SCN (black curve). NH_4^+ and SCN^-

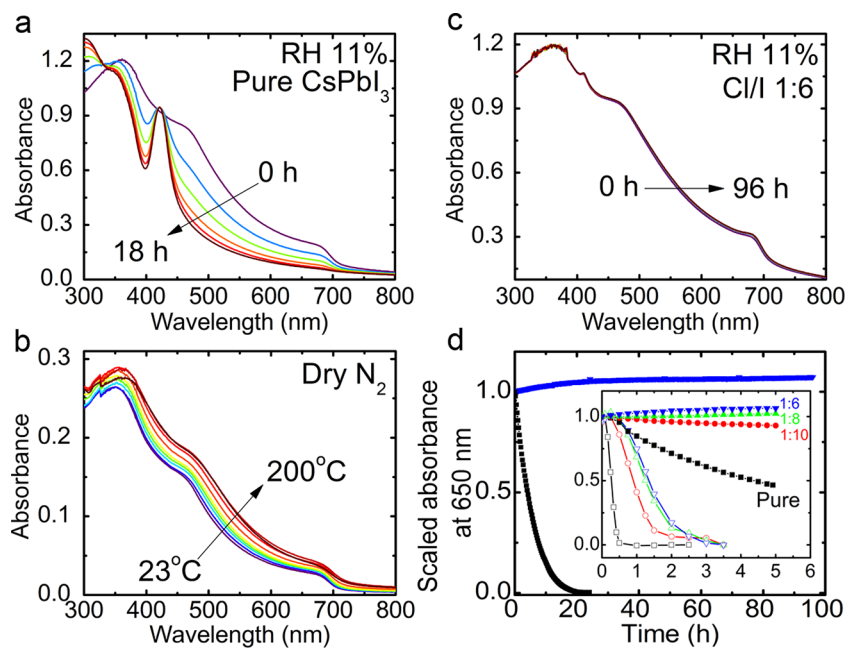


Figure 3. UV-vis absorbance spectra of chemically sintered thin films of pure CsPbI₃ and CsPbI_{3-x}Cl_x. (a) Spectra taken for pure CsPbI₃ over 18 h after exposing the samples to relative humidity (RH) of 11% at 23 °C. (b) Spectra taken for a similarly prepared sample, sealed in a nitrogen atmosphere and heated in situ from 23 to 200 °C over approximately 3 h; individual spectra shown at 20 °C increments. (c) Spectra taken for a mixed film of CsPbCl₃ and CsPbI₃ in a 1:6 nanocrystal number-ratio over 96 h, after exposing the samples to RH of 11% at 23 °C. (d) Normalized absorbance at 650 nm (at which only the perovskite phase absorbs), as a function of time for pure CsPbI₃ and for a mixed film of nanocrystal number ratio of 1:6 CsPbCl₃/CsPbI₃ in black and blue, respectively at RH of 11%. Inset shows additional compositions of 1:10 and 1:8 in red and green, respectively as well as different RH; solid symbols are for samples measured at 11% RH, open symbols at 54% RH. These data indicate the fraction of the sample in the perovskite phase as a function of exposure time to a humid atmosphere.

possess strong infrared transitions due to the N–H and C–N stretches at 3300 and 2100 cm⁻¹, respectively, and the absence of such signatures in the spectrum in black indicates that neither species is adsorbed or incorporated into the nanocrystal solid to an appreciable extent. Soaking the nanocrystals in isopropanol alone can also result in removal of the organic ligands, albeit more slowly (Figure S1a). However, prolonged exposure to isopropanol also results in a transformation of the dark perovskite to a pale yellow material that is spectroscopically distinguishable from the edge-sharing yellow phase (Figure S1b). Thus, the rapid ligand removal that occurs with NH₄SCN makes it possible to remove the ligands while preserving the desired perovskite phase.

In Figure 1d, a transmission electron microscopy (TEM) image of a thin film of CsPbI₃ perovskite nanocrystals is shown after ligand removal, revealing that the smaller nanocrystal precursors have been fused into much larger crystallites. X-ray diffraction (XRD) before and after ligand removal demonstrates that this fusion process preserves the perovskite structure (Figure 2b). The untreated nanocrystals (blue curve) exhibit peaks at approximately 20°, 29°, and 35°, associated with the (110), (200), and (211) directions of the cubic perovskite structure. The diffraction peaks exhibit the broad line widths expected given the small dimensions of the nanocrystals. After ligand removal, crystal grain growth is evident in the narrowing of these peaks (black curve). Close inspection reveals that each of these peaks become split, consistent with a lower symmetry, distorted cubic perovskite structure. This splitting is most clearly seen for the 29° peak (inset). Changes in the electronic structure are observed by UV-vis absorbance spectroscopy upon chemical sintering of the films, shown in Figure 2c. Prior to sintering, a small degree

of size-dependent quantum confinement is observed in the as-made nanocrystals, due to their small dimensions³³ (blue curve). Comparing this to the black curve, the loss of quantum confinement upon sintering leads to a steeper and lower-energy onset of electronic excitations, seen most clearly in the second derivative of the absorbance spectrum, shown in the inset.

Similar to previous studies of bulk-phase CsPbI₃,^{9,11,13} the chemically sintered thin films undergo a rapid phase transition from the perovskite phase to the yellow phase when exposed to a humid atmosphere. This can be readily seen in absorbance spectra (Figure 3a), XRD patterns (Figure S2), and the gross morphology of the films (Figure S3) taken before and after exposure to a humid atmosphere. In the course of 18 h in a 11% relative humidity (RH) atmosphere at 23 °C, this representative sample transforms into a new structure with no long-wavelength absorbance features and a strong absorbance at 420 nm, hence the name “yellow phase”. In contrast, a similarly prepared sample that is sealed under nitrogen is stable in the perovskite phase, not just at room temperature but also at elevated temperature. Absorbance spectra are taken in situ as the sealed sample is heated (Figure 3b) up to 200 °C (the experimental limit of the apparatus) over the course of a few hours. There is no indication of phase change occurring at all under these conditions, despite the availability of abundant thermal energy to facilitate equilibration. Similarly, the analogous CsSnI₃ has been observed to be stable in the perovskite phase for more than a year when stored in an inert atmosphere.^{12,13} The contrast between the spontaneous instability of CsPbI₃ in the presence of water vapor and the robust thermal stability in an inert atmosphere strongly suggests that the role of moisture is not simply to

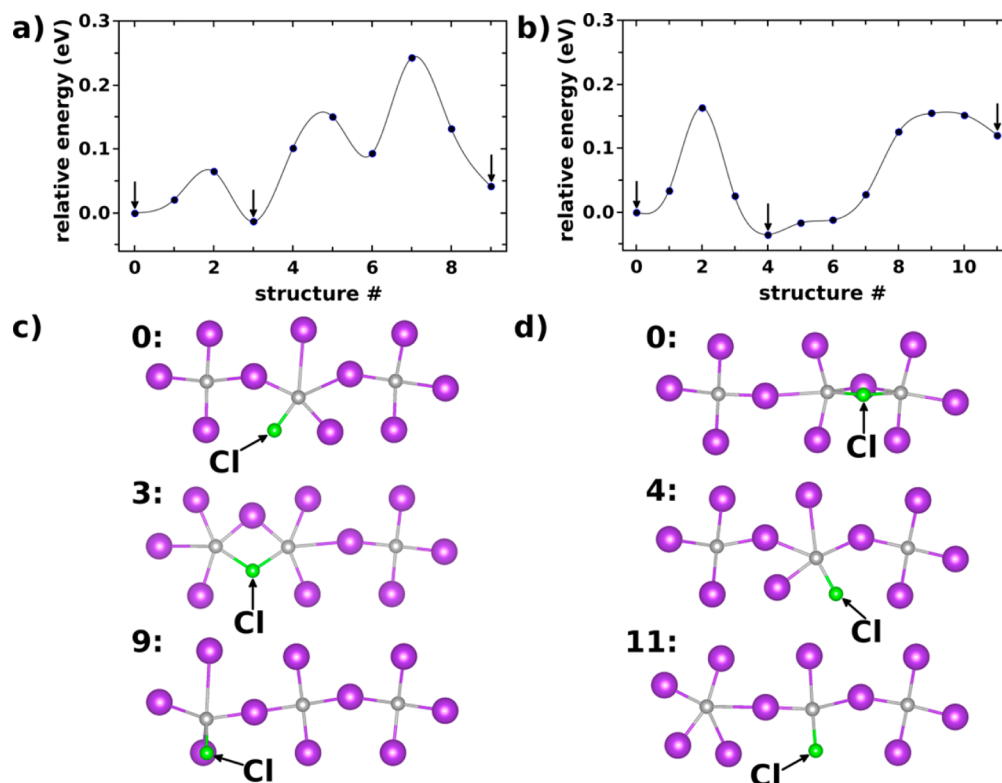


Figure 4. DFT-calculated MEPs for (a) Cl_i (green) migration and (b) anion-exchange reaction of Cl_i with iodide in CsPbI₃. To sample the MEP shown in each panel, we have used two independent NEB calculations that were aligned after separate convergence (at structures 3 and 6 in part a and b, respectively, see SI for details). Symbols represent the energies of images that were used to sample the path and the solid lines are interpolations that serve as a guide to the eye. Panels (c) and (d) show schematic representations of structures along the MEPs, labeled according to the corresponding structure numbers in panels a and b, respectively. The Cl defect is highlighted, Pb atoms are shown in gray, I atoms in purple, and Cs are not shown for simplicity.

lower the kinetic barrier of the phase transition but to perturb the relative free energies of the two phases.

To test whether chloride-doping enhances air-stability of CsPbI₃ films it was necessary to synthesize CsPbI_{3-x}Cl_x thin films. To accomplish this, we mixed colloidal dispersions of CsPbCl₃ and CsPbI₃ nanocrystals and then deposited films. Nanocrystal solid films of 1:10, 1:8, and 1:6 CsPbCl₃/CsPbI₃ nanocrystal-number-ratio were deposited and subsequently chemically sintered using NH₄SCN. For the moment, we defer the question of whether a mixed crystal of CsPbI_{3-x}Cl_x forms or, alternatively, the two phases remain separated on the nanoscale, and instead focus on the air-stability of the films fabricated in this manner. Spectra were taken as a function of time for moisture-exposed samples derived from mixed nanocrystal films. The time scale for the phase transition in a humid atmosphere is strongly retarded by chloride incorporation. Contrasting Figure 3c with 3a, we observe a significant improvement in the stability of chloride-doped films over pure CsPbI₃, employing the same NH₄SCN-induced sintering process in each case. By plotting the relative change in the absorbance at 650 nm, where the perovskite phase absorbs and the yellow phase does not, a comparison can be made between the pure CsPbI₃ sample and those including chloride (Figure 3d). The half-life of the perovskite phase transition for chloride-containing samples is increased by a factor of 6 at 54% RH and by an even greater margin at 11% RH. Instrumental considerations limit the in situ stability study to 96 h (4 days). However, in this interval there is no evidence for the phase transition, compared to a half-life for the pure iodide of

only 5 h under these conditions, indicating an enhancement of at least 2 orders of magnitude at RH 11%.

Multiple chemical arguments can be made for why a CsPbI_{3-x}Cl_x mixed crystal would be more stable in the perovskite phase than the undoped crystal. Chlorine forms a stronger, more directional bond to lead than iodine,⁴⁰ raising the energetic costs of bond rearrangement in the transition to the yellow phase. Indeed, our DFT calculations (see Supporting Information (SI) for details) indicate that chloride-doping increases the bulk modulus from 14.1 to 14.5 GPa. Additionally, the Goldschmidt tolerance factor, a geometric indicator of perovskite stability,⁴¹ predicts greater stability with the smaller-diameter chlorine. For a quantitative understanding of the effect of chlorine on stability, we studied CsPbI_{3-x}Cl_x using DFT. We sought to answer four questions: (1) Is there a driving force for dispersing chloride atoms in the majority-CsPbI₃ phase? (2) Is it kinetically feasible for dispersal to occur at room temperature? (3) Does the stability of the perovskite phase relative to the yellow phase change with chloride-doping? (4) How are the band gap and lattice parameters expected to change as a function of chloride incorporation?

To evaluate the driving force for dispersal of chloride, we calculated with DFT, using the PBE exchange-correlation functional,⁴² the relative stability of the configurations where two chlorides bind to a single lead atom, versus both chloride ions dispersed to different lead atoms. The dispersed state was energetically favored by 0.15 eV, indicating that at least for a small Cl/I molar ratio, dispersing chloride across different lead atoms is thermodynamically favored. These calculations were

performed on all symmetry-inequivalent chloride configurations accessible in a $\sqrt{2} \times \sqrt{2} \times 2$ supercell.

To determine if it is kinetically feasible for the dopant to disperse at room temperature, we have computed a minimum energy path (MEP) for migration of a neutral interstitial chlorine defect (Cl_i) from one octahedron to the neighboring one. To this end, we performed DFT calculations⁴³ and used the climbing-image nudged elastic band (NEB) method^{44,45} to calculate (classical) migration barriers. Local structural minima for starting the NEB calculations as well as optimized lattice constants (vide infra) were obtained with the GADGET tool.⁴⁶ Spin-orbit coupling (SOC) was not considered in the NEB calculations, because its effect was shown to be negligible in calculating the structural properties of lead-halide perovskites⁴⁷ (see Supporting Information for further details). As can be seen from the calculated MEP in Figure 4a and the associated structural changes in Figure 4c, although many different local minima for Cl_i in CsPbI_3 were very similar in energy (see SI for details), Cl_i can bond to Pb. This locally disrupts the Pb–I bonding (structure 0 in Figure 4c). Importantly, however, very little energy (<0.1 eV) is needed to free the Cl_i from its local minimum toward a different local minimum bridging two lead atoms (structure 3 in part c). Consecutive Cl_i migration (structures 3 to 9 in Figure 4c) can occur along curved paths across octahedral faces with a more complex migration profile, involving somewhat higher but still readily accessible activation energies (0.1–0.2 eV). The more complex migration profile is due to intensive atomic rearrangement during Cl_i migration owing to the flexibility of the chemical bonds in lead-halide perovskites. From these results, we conclude that Cl_i diffusion is a fast process in CsPbI_3 . These results provide additional evidence that lead-halide perovskites are mixed electronic-ionic conductors and that several different ionic species can be mobile at room temperature.^{48–56}

In Figure 4b, we show a MEP for an anion exchange reaction, known to be relevant for oxide perovskites⁵⁷ and recently considered for other lead-halide perovskites^{38,39,58–60} as well. For the exchange of an iodide in the perovskite lattice by Cl_i , we find that only a small energy barrier of less than 0.2 eV is involved (see Figure 4b,d). This shows that halide exchange occurs on a fast time scale and that chlorine can easily be integrated into the lead-halide perovskite framework (see Figure 4d). The iodine interstitial defect (I_i) resulting from this process appears to be slightly lower in energy (by ca. 0.1 eV) closer to the chloride site than in the neighboring PbI_6 octahedron. Nevertheless, the forward barrier for I_i migration is very small (0.15 eV) so that I_i is likely to move fast as well, similar to what has been reported for the case of MAPbI_3 .⁵⁴ In summary, diffusion of chlorine and incorporation into the perovskite host should be facile at room temperature.

To evaluate the stability of the mixed crystal, the energies of the perovskite and yellow phases were evaluated by DFT for pure CsPbI_3 , pure CsPbCl_3 , and mixed structures at 1:5 and 1:11 Cl/I molar ratio (see Figure S4). At $T = 0$ K, the yellow phase was favored by 0.048 eV for pure CsPbI_3 and by 0.024–0.051 eV for the uniformly doped crystal (depending on configuration), while the perovskite phase was favored by 0.070 eV for pure CsPbCl_3 per formula unit. At finite temperatures, entropic considerations become important and calculation of the vibrational entropy within the harmonic approximation is required. For pure CsPbI_3 , the calculated equilibrium changes to favor the perovskite phase over the yellow phase at 200 K and above, which is consistent with the experimental

equilibrium under nitrogen (Figure 3b). Specifically, the perovskite phase is favored by 0.034 eV per formula unit at room temperature. The calculated equilibrium structure for pure CsPbCl_3 was the perovskite phase at all temperatures. Entropic considerations for the mixed crystal displayed complex behavior, favoring the perovskite phase in some configurations and favoring the yellow phase in others (see Supporting Information for details). In summary, although there are some configurations and temperatures for which the $\text{CsPbI}_{3-x}\text{Cl}_x$ perovskite phase is favored over the yellow phase, the calculations do not provide strong evidence for a direct stabilizing effect of chloride at the calculated doping levels. To understand the role chloride plays in the experimentally observed stability, we sought a more complete model of how chloride is distributed in the films, focusing in particular on the presence of segregated CsPbCl_3 domains.

In the previous section, DFT calculations on the driving force and kinetics of diffusion indicate that once incorporated chloride will tend to disperse in a majority- CsPbI_3 phase. However, this was only for low doping levels and the miscibility of chloride has not been explicitly calculated. Experimental precedent would suggest that it is small.⁶¹ Recently, Kovalenko and co-workers,^{33,38} and independently Akkerman et al.,³⁹ demonstrated that colloidal nanocrystals of CsPbX_3 can be synthesized for Br/I and Br/Cl but not Cl/I alloys. The latter group made the remarkable observation that in colloidal dispersions consisting of a mixture of two pure CsPbX_3 nanocrystal types, for example, CsPbCl_3 and CsPbBr_3 , rapid anion exchange occurs at room temperature to form a single population of alloyed $\text{CsPb}(\text{Cl}/\text{Br})_3$ nanocrystals. However, it was reported that alloys did not form for the Cl/I combination, which was attributed by the authors to the immiscibility of these two halides due to their size mismatch. In the present work, when a colloidal mixture of CsPbCl_3 and CsPbI_3 in a 1:6 number ratio was prepared and the absorbance measured, as shown in Figure 5, the spectrum (black) resembles a

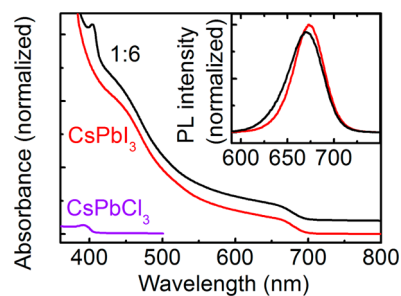


Figure 5. UV–vis absorbance and photoluminescence spectra of nanocrystals in solution. CsPbCl_3 (purple), CsPbI_3 (red), and a 1:6 mixture $\text{CsPbCl}_3/\text{CsPbI}_3$ (black) solutions of nanocrystals in octane are shown. The 1:6 $\text{CsPbCl}_3/\text{CsPbI}_3$ spectrum has been offset and the pure CsPbCl_3 spectrum has been scaled to an equivalent concentration of the CsPbCl_3 nanocrystal fraction in the 1:6 mixture. Inset shows the photoluminescence spectra, which have been scaled to an equivalent absorption at the excitation wavelength of 500 nm to afford a comparison of their relative quantum yield.

superposition of the spectra of two independent populations of nearly unperturbed CsPbCl_3 and CsPbI_3 nanocrystals (purple and red, respectively). Similarly, the photoluminescence spectrum of the mixture was also measured, as shown in the inset to Figure 5, (black) and little change in peak energy or quantum yield was observed relative to the pure CsPbI_3

nanocrystals (red). Close inspection reveals that the band-edge absorbance peak associated with the CsPbCl_3 shifts slightly from 393 to 404 nm and the photoluminescence of CsPbI_3 shifts from 673 to 670 nm when mixed. This evidence suggests that only a small amount of anion mixing occurs in solution for Cl and I if any, which is consistent with previous reports.^{38,39}

However, a fraction of the chloride present as CsPbCl_3 in the as-deposited mixed films partitions into the majority- CsPbI_3 phase during the chemical sintering process, rendering it doped. This is evidenced by two experimental observables: changes in band gap measured by the electronic absorbance spectrum and the crystallographic lattice parameters measured by XRD (Table 1). However, a priori we do not know the quantitative

Table 1. Calculated and Measured Effects of Chloride Incorporation

chloride mole fraction $\text{Cl}/[\text{Cl} + \text{I}] \times 100$ (Cl/I)	volume contraction $-\Delta V/V$	change in band gap ^a [eV]
Theoretical		
2.1% (1:47)	0.6%	0.03
4.3% (1:23)	1.2%	0.04
9.1% (1:10)	1.7%	0.09
Experimental		
9% (1:10)	0.6%	0.03 ± 0.01
11% (1:8)	0.6%	0.02 ± 0.01
14% (1:6)	0.6%	0.02 ± 0.01

^aCalculated relative to pure CsPbI_3 .

correlation between these parameters and the value of x in the putative $\text{CsPbI}_{3-x}\text{Cl}_x$ phase. To calibrate this correlation, we performed DFT calculations of both parameters as a function of chloride-fraction (Table 1). Overall, we find that chloride changes the band gap only to a small extent. In these calculations, SOC is treated fully self-consistently for greater accuracy in the calculated electronic structure;⁶² without SOC, the effect is even smaller. The minor effect of chloride incorporation can be explained by the fact that the electronic states due to chloride in CsPbI_3 do not contribute to the frontier states in the band structure (see Figure S5), as the ionization potential of chlorine is larger than that of iodine.

Comparing the calculated data to experimental results, shifts in the band gap on the order of 20 meV are observed for all of the mixed nanocrystal samples, as shown in Table 1. Within our experimental uncertainty, this does not vary with increasing number-ratio of CsPbCl_3 nanocrystals. Although it may be anticipated that the change in band gap could also be measured by photoluminescence, no detectable photoemission above the instrumental background was observed after NH_4SCN treatment. By comparing the XRD patterns of pure, sintered CsPbI_3 and the sintered, mixed samples (Supporting Figure S6), the change in the 2θ values of the bifurcated peaks at 29° that are derived from the cubic (002) peak indicate a volume contraction of approximately 0.6% in the putative $\text{CsPbI}_{3-x}\text{Cl}_x$ phase for all cases. The best agreement between the calculated and measured changes in band gap and lattice volume occurs for an assumed chloride mole-fraction of approximately 2% in the majority phase. This is much lower than the average mole ratio in the deposited solution, implying that some of the chloride is not incorporated and remains segregated in the film in CsPbCl_3 domains. It is interesting to note that the amount of chloride present in the mixed film and its effect on the band gap and lattice parameters are similar to the results of calculations

of chloride incorporation in the hybrid perovskites.³¹ Furthermore, it should be noted that, unlike the hybrid perovskites, in the present system there is no volatile component that by evaporating can change the overall stoichiometry of the film.⁶³

The discrepancy between the amount of chloride in the mixture prior to sintering, based on the nanocrystal-number-fraction, and the small doping levels indicated in the previous section can be directly accounted for in the form of segregated perovskite-phase CsPbCl_3 inclusions in the sintered films. These are identified by their distinct spectral signature at approximately 410 nm due to the onset of above-band gap excitation. Figure 6 shows this region for samples of nanocrystal

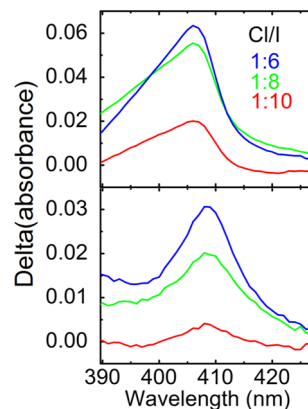


Figure 6. UV-vis absorbance spectra of mixtures of $\text{CsPbCl}_3/\text{CsPbI}_3$ nanocrystals after subtracting a pure CsPbI_3 reference spectrum, showing the characteristic absorption feature for perovskite-phase CsPbCl_3 . (a) Pristine, mixed nanocrystal films, as deposited. (b) Mixed nanocrystal films after chemical sintering with NH_4SCN . Nanocrystal number ratios of 1:6, 1:8, and 1:10 are in blue, green, and red, respectively.

films as deposited (Figure 6a) and the films after sintering (Figure 6b) after subtracting a pure CsPbI_3 reference spectrum, which possesses no feature at 410 nm. With increasing nanocrystal number-fraction, the signature 410 nm peak due to CsPbCl_3 band gap absorption is seen to increase in the as-deposited films. After sintering, the integrated area of the peak associated with the chloride phase decreases relative to the pristine mixed films, for all compositions. This is consistent with a repartitioning of a fraction of the chloride from the CsPbCl_3 nanocrystals in to the mixed $\text{CsPbI}_{3-x}\text{Cl}_x$ majority phase induced by sintering, thereby achieving the doping levels indicated by the band edge shift and lattice contraction in Table 1. However, even the 1:10 sample continues to exhibit a detectable amount of absorbance associated with the CsPbCl_3 phase. This indicates that indeed some quantity of CsPbCl_3 remains in the chemically sintered films as unmixed inclusions in all cases. This fact, combined with the observations that the band gap and lattice parameters in the $\text{CsPbI}_{3-x}\text{Cl}_x$ majority phase are all similarly perturbed at each of the doping levels explored (Table 1), suggests that above a chloride/iodide ratio of 1:10, most of the additional chloride remains segregated. Nonetheless, the stability is further enhanced at these higher chloride/iodide ratios (Figure 3d). Considering that the DFT calculations do not indicate a stabilizing effect of uniform chloride doping on the formation energy of the $\text{CsPbI}_{3-x}\text{Cl}_x$ perovskite phase, we speculate that the film structure, consisting of a majority of mixed polycrystalline $\text{CsPbI}_{3-x}\text{Cl}_x$

alongside a small concentration of CsPbCl₃ crystallites, may have more to do with the enhanced stability of these films.

Conclusions. We conclude that a mixed polycrystalline thin film of CsPbI_{3-x}Cl_x is the product of chemically sintering mixed nanocrystal films. On the basis of the comparison between experimental and DFT calculated values of the band gap and lattice parameters, the CsPbI_{3-x}Cl_x majority phase consists of a mole-fraction in the range of 2%. This appears to be an upper limit on the extent of chloride incorporation in the iodide-majority lattice, regardless of the nanocrystal number ratio, and the excess chloride beyond this limit remains as CsPbCl₃-phase inclusions. In this configuration, the films exhibit an enhanced stability toward phase change in humid conditions relative to the undoped state. Likely this effect is not explained simply by an increased energetic stability of a homogeneous mixed-crystal. Nonetheless, this represents a new approach to stabilizing the functional phase of CsPbI₃ and may prove to be a critical step forward in enabling the use of this material, and possibly related ones, for device applications.

■ ASSOCIATED CONTENT

Supporting Information

The Supporting Information is available free of charge on the ACS Publications website at DOI: 10.1021/acs.nanolett.6b00635.

Detailed experimental and calculation procedures, additional XRD and SEM figures, and calculated density of states. (PDF)

■ AUTHOR INFORMATION

Corresponding Author

*E-mail: fafarman@drexel.edu.

Author Contributions

The manuscript was written through contributions of all authors. All authors have given approval to the final version of the manuscript.

Notes

The authors declare no competing financial interest.

■ ACKNOWLEDGMENTS

S.D., A.D.D., and A.T.F. acknowledge support from Drexel University. D.A.E. and L.K. were supported by a research grant from Dana and Yossie Hollander, by the Lise Meitner Minerva Center for Computational Chemistry, and by the Austrian Science Fund (FWF): J3608-N20. S.L. is supported by Carnegie Institution for Science. L.Z.T. acknowledges support from the Office of Naval Research, under Grant N00014-14-1-0761. A.M.R. acknowledges support from the Department of Energy Office of Basic Energy Sciences, under Grant DE-FG02-07ER46431. The authors acknowledge computational support from the HPCMO of the DoD and the NERSC of the DOE.

■ ABBREVIATIONS

DFT, density functional theory; MA, methylammonium; RH, relative humidity; XRD, X-ray diffraction; UV–vis, ultraviolet–visible; FTIR, Fourier transform infrared; MEP, minimum energy path; Cl_i, interstitial chlorine; PBE, Perdew–Burke–Ernzerhof; NEB, nudged elastic band

■ REFERENCES

- (1) Brenner, T. M.; Egger, D. A.; Kronik, L.; Hodes, G.; Cahen, D. *Nat. Rev. Mater.* **2016**, *1*, 15007.
- (2) Kojima, A.; Teshima, K.; Shirai, Y.; Miyasaka, T. *J. Am. Chem. Soc.* **2009**, *131*, 6050–6051.
- (3) Yang, W. S.; Noh, J. H.; Jeon, N. J.; Kim, Y. C.; Ryu, S.; Seo, J.; Seok, S. I. *Science* **2015**, *348*, 1234–1237.
- (4) Lee, M. M.; Teuscher, J.; Miyasaka, T.; Murakami, T. N.; Snaith, H. J. *Science* **2012**, *338*, 643–647.
- (5) Cheng, Z.; Lin, J. *CrystEngComm* **2010**, *12*, 2646–2662.
- (6) Noh, J. H.; Im, S. H.; Heo, J. H.; Mandal, T. N.; Seok, S. I. *Nano Lett.* **2013**, *13*, 1764–1769.
- (7) Misra, R. K.; Aharon, S.; Li, B.; Mogilyansky, D.; Visoly-Fisher, I.; Etgar, L.; Katz, E. A. *J. Phys. Chem. Lett.* **2015**, *6*, 326–330.
- (8) Niu, G.; Li, W.; Meng, F.; Wang, L.; Dong, H.; Qiu, Y. *J. Mater. Chem. A* **2014**, *2*, 705–710.
- (9) Møller, C. K. *Nature* **1958**, *182*, 1436–1436.
- (10) Eperon, G. E.; Paternò, G. M.; Sutton, R. J.; Zampetti, A.; Haghighirad, A. A.; Cacialli, F.; Snaith, H. J. *J. Mater. Chem. A* **2015**, *3*, 19688–19695.
- (11) Trots, D. M.; Myagkota, S. V. *J. Phys. Chem. Solids* **2008**, *69*, 2520–2526.
- (12) Chung, I.; Song, J.-H.; Im, J.; Androulakis, J.; Malliakas, C. D.; Li, H.; Freeman, A. J.; Kenney, J. T.; Kanatzidis, M. G. *J. Am. Chem. Soc.* **2012**, *134*, 8579–8587.
- (13) Stoumpos, C. C.; Malliakas, C. D.; Kanatzidis, M. G. *Inorg. Chem.* **2013**, *52*, 9019–9038.
- (14) Ripolles, T. S.; Nishinaka, K.; Ogomi, Y.; Miyata, Y.; Hayase, S. *Sol. Energy Mater. Sol. Cells* **2016**, *144*, 532–536.
- (15) Kulbak, M.; Cahen, D.; Hodes, G. *J. Phys. Chem. Lett.* **2015**, *6*, 2452–2456.
- (16) Kulbak, M.; Gupta, S.; Kedem, N.; Levine, I.; Bendikov, T.; Hodes, G.; Cahen, D. *J. Phys. Chem. Lett.* **2016**, *7*, 167–172.
- (17) Li, Z.; Yang, M.; Park, J.-S.; Wei, S.-H.; Berry, J. J.; Zhu, K. *Chem. Mater.* **2016**, *28*, 284–292.
- (18) Li, W.; Li, J.; Niu, G.; Wang, L. *J. Mater. Chem. A* **2015**, DOI: 10.1039/C5TA09165A.
- (19) Lee, J.-W.; Kim, D.-H.; Kim, H.-S.; Seo, S.-W.; Cho, S. M.; Park, N.-G. *Adv. Energy Mater.* **2015**, *5*, 1501310.
- (20) McMeekin, D. P.; Sadoughi, G.; Rehman, W.; Eperon, G. E.; Saliba, M.; Hörlantner, M. T.; Haghighirad, A.; Sakai, N.; Korte, L.; Rech, B.; Johnston, M. B.; Herz, L. M.; Snaith, H. J. *Science* **2016**, *351*, 151–155.
- (21) Beal, R. E.; Slotcavage, D. J.; Leijtens, T.; Bowring, A. R.; Belisle, R. A.; Nguyen, W. H.; Burkhard, G.; Hoke, E. T.; McGehee, M. D. *J. Phys. Chem. Lett.* **2016**, *7*, 746.
- (22) Sutton, R. J.; Eperon, G. E.; Miranda, L.; Parrott, E. S.; Kamino, B. A.; Patel, J. B.; Hörlantner, M. T.; Johnston, M. B.; Haghighirad, A. A.; Moore, D. T.; Snaith, H. J. *Adv. Energy Mater.* **2016**, *6*, 6.
- (23) Fujii, Y.; Hoshino, S.; Yamada, Y.; Shirane, G. *Phys. Rev. B* **1974**, *9*, 4549–4559.
- (24) Chae, J.; Dong, Q.; Huang, J.; Centrone, A. *Nano Lett.* **2015**, *15*, 8114–8121.
- (25) Colella, S.; Mosconi, E.; Fedeli, P.; Listorti, A.; Gazza, F.; Orlandi, F.; Ferro, P.; Besagni, T.; Rizzo, A.; Calestani, G.; Gigli, G.; De Angelis, F.; Mosca, R. *Chem. Mater.* **2013**, *25*, 4613–4618.
- (26) Colella, S.; Mosconi, E.; Pellegrino, G.; Alberti, A.; Guerra, V. L. P.; Masi, S.; Listorti, A.; Rizzo, A.; Condorelli, G. G.; De Angelis, F.; Gigli, G. *J. Phys. Chem. Lett.* **2014**, *5*, 3532–3538.
- (27) Dar, M. I.; Arora, N.; Gao, P.; Ahmad, S.; Grätzel, M.; Nazeeruddin, M. K. *Nano Lett.* **2014**, *14*, 6991–6996.
- (28) Li, Y.; Sun, W.; Yan, W.; Ye, S.; Peng, H.; Liu, Z.; Bian, Z.; Huang, C. *Adv. Funct. Mater.* **2015**, *25*, 4867–4873.
- (29) Unger, E. L.; Bowring, A. R.; Tassone, C. J.; Pool, V. L.; Gold-Parker, A.; Checharoen, R.; Stone, K. H.; Hoke, E. T.; Toney, M. F.; McGehee, M. D. *Chem. Mater.* **2014**, *26*, 7158–7165.
- (30) Dualeh, A.; Tétreault, N.; Moehl, T.; Gao, P.; Nazeeruddin, M. K.; Grätzel, M. *Adv. Funct. Mater.* **2014**, *24*, 3250–3258.

- (31) Mosconi, E.; Amat, A.; Nazeeruddin, M. K.; Grätzel, M.; De Angelis, F. *J. Phys. Chem. C* **2013**, *117*, 13902–13913.
- (32) Sabba, D.; Mulmudi, H. K.; Prabhakar, R. R.; Krishnamoorthy, T.; Baikie, T.; Boix, P. P.; Mhaisalkar, S.; Mathews, N. *J. Phys. Chem. C* **2015**, *119*, 1763–1767.
- (33) Protesescu, L.; Yakunin, S.; Bodnarchuk, M. I.; Krieg, F.; Caputo, R.; Hendon, C. H.; Yang, R. X.; Walsh, A.; Kovalenko, M. V. *Nano Lett.* **2015**, *15*, 3692–3696.
- (34) Ruess, R.; Benfer, F.; Böcher, F.; Stumpp, M.; Schlettwein, D. *ChemPhysChem* **2016**, DOI: [10.1002/cphc.201501168](https://doi.org/10.1002/cphc.201501168).
- (35) Zheng, F.; Takenaka, H.; Wang, F.; Koocher, N. Z.; Rappe, A. M. *J. Phys. Chem. Lett.* **2015**, *6*, 31–37.
- (36) Sharma, S.; Weiden, N.; Weiss, A. *Z. Phys. Chem.* **1992**, *175*, 63–80.
- (37) Pistor, P.; Borchert, J.; Fränzel, W.; Csuk, R.; Scheer, R. *J. Phys. Chem. Lett.* **2014**, *5*, 3308–3312.
- (38) Nedelcu, G.; Protesescu, L.; Yakunin, S.; Bodnarchuk, M. I.; Grotevent, M. J.; Kovalenko, M. V. *Nano Lett.* **2015**, *15*, 5635–5640.
- (39) Akkerman, Q. A.; D’Innocenzo, V.; Accornero, S.; Scarpellini, A.; Petrozza, A.; Prato, M.; Manna, L. *J. Am. Chem. Soc.* **2015**, *137*, 10276–10281.
- (40) Sun, S.; Fang, Y.; Kieslich, G.; White, T. J.; Cheetham, A. K. *J. Mater. Chem. A* **2015**, *3*, 18450–18455.
- (41) Goldschmidt, V. M. *Naturwissenschaften* **1926**, *14*, 477–485.
- (42) Perdew, J. P.; Burke, K.; Ernzerhof, M. *Phys. Rev. Lett.* **1996**, *77*, 3865–3868.
- (43) Kresse, G.; Furthmüller, J. *Phys. Rev. B: Condens. Matter Mater. Phys.* **1996**, *54*, 11169–11186.
- (44) Henkelman, G.; Uberuaga, B. P.; Jónsson, H. *J. Chem. Phys.* **2000**, *113*, 9901–9904.
- (45) Henkelman, G.; Jónsson, H. *J. Chem. Phys.* **2000**, *113*, 9978–9985.
- (46) Bučko, T.; Hafner, J.; Ángyán, J. G. *J. Chem. Phys.* **2005**, *122*, 124508.
- (47) Egger, D. A.; Kronik, L. *J. Phys. Chem. Lett.* **2014**, *5*, 2728–2733.
- (48) Dualeh, A.; Moehl, T.; Tétreault, N.; Teuscher, J.; Gao, P.; Nazeeruddin, M. K.; Grätzel, M. *ACS Nano* **2014**, *8*, 362–373.
- (49) Yang, T.-Y.; Gregori, G.; Pellet, N.; Grätzel, M.; Maier, J. *Angew. Chem.* **2015**, *127*, 8016–8021.
- (50) Yuan, Y.; Chae, J.; Shao, Y.; Wang, Q.; Xiao, Z.; Centrone, A.; Huang, J. *Adv. Energy Mater.* **2015**, *5*, 1500615.
- (51) Eames, C.; Frost, J. M.; Barnes, P. R. F.; O’Regan, B. C.; Walsh, A.; Islam, M. S. *Nat. Commun.* **2015**, *6*, 7497.
- (52) Yuan, Y.; Wang, Q.; Shao, Y.; Lu, H.; Li, T.; Gruverman, A.; Huang, J. *Adv. Energy Mater.* **2016**, *6*, 1501803.
- (53) Eperon, G. E.; Beck, C. E.; Snaith, H. J. *Mater. Horiz.* **2016**, *3*, 63–71.
- (54) Azpiroz, J. M.; Mosconi, E.; Bisquert, J.; De Angelis, F. *Energy Environ. Sci.* **2015**, *8*, 2118–2127.
- (55) Haruyama, J.; Sodeyama, K.; Han, L.; Tateyama, Y. *J. Am. Chem. Soc.* **2015**, *137*, 10048–10051.
- (56) Egger, D. A.; Kronik, L.; Rappe, A. M. *Angew. Chem., Int. Ed.* **2015**, *54*, 12437–12441.
- (57) Dutton, S. E.; Hirai, D.; Cava, R. J. *Mater. Res. Bull.* **2012**, *47*, 714–718.
- (58) Palazon, F.; Akkerman, Q. A.; Prato, M.; Manna, L. *ACS Nano* **2016**, *10*, 1224–1230.
- (59) Pellet, N.; Teuscher, J.; Maier, J.; Grätzel, M. *Chem. Mater.* **2015**, *27*, 2181–2188.
- (60) Jang, D. M.; Park, K.; Kim, D. H.; Park, J.; Shojaei, F.; Kang, H. S.; Ahn, J.-P.; Lee, J. W.; Song, J. K. *Nano Lett.* **2015**, *15*, 5191–5199.
- (61) Belyaev, I. N.; Shurginov, E. A. *Russ. J. Inorg. Chem.* **1970**, *15*, 719–721.
- (62) Even, J.; Pedesseau, L.; Jancu, J.-M.; Katan, C. *J. Phys. Chem. Lett.* **2013**, *4*, 2999–3005.
- (63) Pool, V. L.; Gold-Parker, A.; McGehee, M. D.; Toney, M. F. *Chem. Mater.* **2015**, *27*, 7240–7243.

■ NOTE ADDED AFTER ASAP PUBLICATION

This paper was published on the Web on May 13, 2016. Figures 1 and 2 were increased in size, and the corrected version was reposted on May 17, 2016.